Dynamics of long hyaluronic acid chains through conical nanochannels for characterizing enzyme reactions in confined spaces

Tianji Ma, Jean-Marc Janot, Sebastien Balme

Dynamics of Long Hyaluronic Acid Chains through Conical Nanochannel for Characterizing Enzyme Reactions in Confined Space

Tianji Ma[a], Jean-Marc Janot[a], Sébastien Balme*[a]

This research reports the transport behaviors of long flexible polymers (hyaluronic acids) through long conical track-etched nanochannels with and without grafted enzymes. The impacts of the channel diameter as well as the polymer regimes in solution (dilute and semi-dilute) have been investigated. Without enzymes, the experimental results can be well explained by the analytical models of the scaling law of de Gennes. Then, the corresponding enzymes (hyaluronidase) are grafted inside the channel. When enzymes are located in the base side, polymers get degraded at the entrance and degraded products were detected. When enzymes are grafted at the tip side, the extension of translocation duration due to the binding of substrate-enzyme is observed. This is for the first time that the enzymatic degradation reactions are characterized *in situ* at single molecule level by nanopore technology.

Introduction

Enzymes as a biological catalyst play a vital role in living cells to accelerate chemical reactions in life conditions. The efficiency of enzymes comes from their highly precise and complex structures as well-designed machines. They find numerous applications in food industries, fine chemical synthesis and waste treatment from lab to industrial scale[1]. The enzymatic reactions can be performed under porous materials to design enzymatic membrane reactors (EMR)[2]. To this purpose, the enzymes were immobilized via physical adsorption, entrapment or covalent bonding in numerous porous materials[3,4] such as silica[5], clay minerals[6], double layered hydroxides[7], aluminum oxide[8], celites[9], agarose[10], polyelectrolytes[11] and metal-organic frameworks[12,13] according to enzyme properties and reaction conditions. The enzymatic reactions have been proved to be well carried out in porous membranes by confirming satisfied products output[1]. However, much effort has to be done to understand what exactly happens when an enzyme is immobilized in a confined space. More than 100 years ago, Leonor Michaelis and Maud Leonora Menten proposed an equation (so-called Michaelis-Menten) to describe enzymatic reaction kinetics[14]: $E + S \underset{k_{-1}}{\overset{k_1}{\rightleftarrows}} E \times S \xrightarrow{k_{cat}} E + P$ where k_1 and k_{-1} are the forward and reverse rate constants for substrate binding and k_{cat} is the catalytic rate constant. The k_{cat} is well confirmed by ensemble experiments, whereas, for each enzyme reaction, it should be different because of the general existence of fluctuations which is hidden at the ensemble level[15]. The recent advanced techniques based on fluorescence imaging microscopy and spectroscopy, as well as molecule manipulations make it possible to further characterization of the enzymatic reactions at single molecule level[16–18]. These techniques allow the real time observation of each step and intermediates involved during enzymatic reaction. However, spectroscopy based techniques are limited to study enzymes under confined space.

Nanopore technology is found as good way to investigate biochemical reaction[19,20]. On the one hand, the kinetic of enzymatic reactions have been characterized by ensemble experiments using both proteins and solid-state nanopores. Fennouri et *al*. achieved the characterization of enzyme activity by study of the translocation of degraded hyaluronic acid through biological nanopore[21,22]. Using track-etched nanopore, our group followed the enzymatic degradation of β-lactoglobulin amyloid by resistive pulse technique[23] and heparin by ionic current rectification[24]. On the other hand, by immobilizing proteins inside single solid-state nanopores several groups achieved to detect specific bindings using resistive pulse technique. Wei et *al*. immobilized protein A (his-6-tragged) on nitrilotriacetic acid (NTA)-moieties attached to a gold-coated silicon nitride (SiN) nanopore and the kinetics of IgG antibody binding to Protein A was observed[25]. Yusko EC et *al*. immobilized biotin molecules on a lipid bilayer coated SiN nanopore[26]. Then, streptavidin was detected through the pore, resulting from the specific biotin-avidin interaction. In addition to protein measurement, plug-docking approach also has been widely used in single molecule dynamics. Shi et *al.* docked a protein-DNA complex into a solid-state nanopore makes it possible to detect conformational changes of a tethered DNA molecule[27].Inspired by these previous works, we can hypothesize that nanopore approach is a suitable way to study enzyme activity directly inside a nanopore. We expect combine (i) the real-time analysis of enzymatic degradation products and (ii) characterization of enzyme-substrate interaction by measuring translocation duration change.

Before characterizing the enzymatic reaction, inside a nanopore we should well understand the whole process of the flexible polymers flowing into a confined space. This was investigated by theoretical studies and simulations since more than 40 years[28]. De Gennes and co-workers have proposed scaling theory for describing flexible polymers under confined space using Pincus' blob model. This called de Gennes' regime is different from Odijk's where channel/pore diameter h is smaller than twice of persistence length of the molecule a ($h < 2a$)[29]. De Gennes' regime describes the cases where channel

(or pore) diameter *D* is larger than 2*a* but still smaller than the coil diameter of polymers in bulk *D* (2*a* < *h* < *D*). In this regime, polymers can be considered as a series of blobs which contain a number of monomers. Peterlin, de Gennes and Pincus successively proposed and calculated a critical volumetric flow where a coil-like polymer would change to a stretched form in a nanopore[30–32]. Based on that, Daoudi et *al*. described flexible polymers flowing inside conical channels by identifying dilute regime and semi-dilute regime according to a possible overlap of polymer coils in bulk solution[33]. On the same way in developing de Gennes' regime in conical nanochannel, relations between the number of monomers and the axis distance occupied in a defined conical channel was established[34,35]. Theoretical studies are far ahead of related experimental research due to the difficulty in preparing well-defined samples providing related confined space in nanoscale[36]. From 1990s, the progress in single nanopore technology[37] for single molecule sensing[38] draws more research interests on that especially to investigate voltage driven translocations. Numerous experiments of voltage-driven polymer translocations through different kinds of asymmetric nanopore such as proteins[14,15,18,39–41], nanocapillaries[42–44] and polymer track-etched[45] have been done However, there was never reported the experiments of translocating a large enough macromolecule in a conical channel with small enough tip aperture under de Gennes' regime which are similar to conditions of above theoretical studies.

This paper aims to investigate the enzymatic degradation of the polymer (the hyaluronic acid noted as HA) with high molecular weight (1.5 MDa < M < 1.8 MDa) directly inside the conical nanochannel at single molecule level. We first investigate the translocation of HA through conical track-etched nanochannels under dilute and semi-dilute regimes since such study is still missing. In that case, we aim to make an experimental evidence of the blobs model of flexible polymer inside conical channel. Then hyaluronidase was immobilized on the channel inner wall by a one-step chemical bonding. By controlling enzyme positions only in base side of the conical channel, a real-time analysis of enzymatic degradation was achieved. Finally, the grafting of enzymes in the narrowest of the channel (tip side) made possible the measurement of the translocation duration changes to identify the enzyme-substrate mechanism.

Results and discussions

Influence of the regime on HA translocation through conical nanochannel.

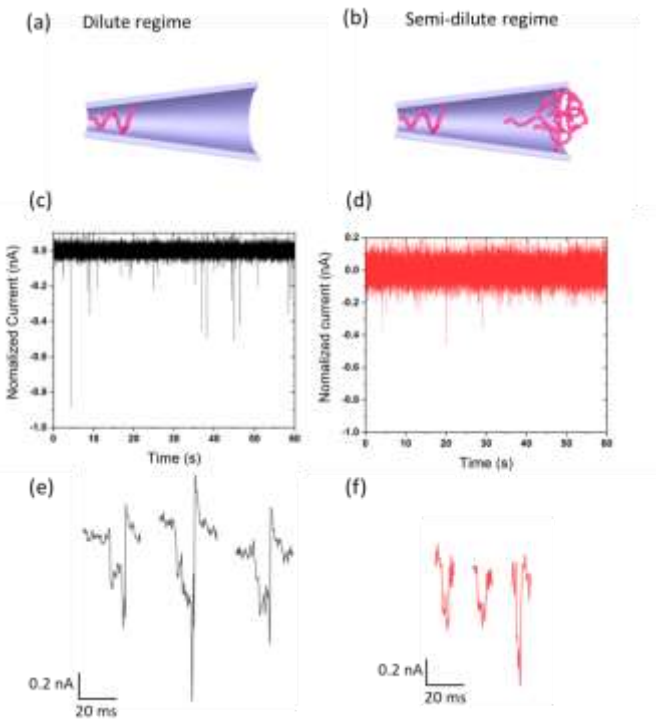

Fig. 1 Sketch representations of hyaluronic acid through conical channel in dilute regime (a) and in semi-dilute regime (b). The sketches are not to scale. Examples of current trace recorded in dilute regime (c) and semi-dilute regime (d). Zoom of current blockade in dilute regime (e) and in the semi-dilute regime (f). Channel 1 in black: D_{base} = 715 nm, D_{tip} = 23.5 nm and Channel 2 in red: D_{base} = 750 nm, D_{tip} = 35.4 nm.

The single conical nanochannel in polymer film was fabricated by track-etching method under asymmetric condition [46]. It was mounted in a cell composed by two chambers filled with phosphate saline buffer (PBS) where NaCl concentration was adjusted to 1 M. For experiments in the dilute regime and semi-dilute regime, two similar conical nanochannels (L= 13 µm) were used with base and tip diameters at D_{base} = 715 nm, D_{tip} = 23.5 nm (α = 1.52°) (noted as nanochannel 1) and at D_{base} = 750 nm D_{tip} = 35.4 nm (α = 1.57°) (noted as nanochannel 2) respectively. Detailed characterization of four nanochannels used in experiments can be found in Figure S1. Hyaluronic acid with a high molar weight between 1.5 to 1.8 10^6 g mol^{-1} has a large hydrodynamic diameter which was estimated between 280 nm to 310 nm under physiological saline solution according to literature[47]. With such molar weight, the number of monomers N in a hyaluronic chain can be calculated between 3858 and 4749. Considering the number of monomers ($N \approx 4350$), the stretched chain length is estimated to 4000 nm (monomer length a=1.1 nm). To switch from dilute to semi-dilute regime, hyaluronic acid should have a strong interaction between each other. Under 1 M NaCl and according to the polymer size, the critical concentration ($c^* = a^{-3}N^{-\frac{4}{5}}$) of hyaluronic acid is estimated 500 nM from de Gennes'and Cowman's theories[34,47]. Considering that, we performed translocation experiments at 120 nM or 600 nM of hyaluronic acid for nanochannel 1 (dilute regime) and nanochannel 2 (semi-dilute regime) respectively. The hyaluronic acid was added on the base side and

transmembrane biases from 300 mV to 900 mV were applied to drive polymers approaching, being captured and passing through the nanochannel. As our nanochannels have a conical shape and a base diameter more than twice larger than the hydrodynamic diameter of polymers, we can assume that the polymer entrance inside the channel requires overcoming a low energy barrier[48,49].

Figure 1a and b depict the schematic representations of the polymers inside the conical nanochannels. Examples of current traces recorded at 700 mV during 10 s for polymers in two different regimes are shown in Figure 1c and d with a zoom of several current blockades (Figure 1e and f). We can observe that the shapes of current blockades are different for the two regimes. In dilute one, the blockades show a clear asymmetric shape with a ΔI_{max} value at the end of the event. This shape-depending signal can be referring to the chain coil compression from base side to tip side in a conical channel (Figure S2). In other words, the density of the coil gets increased during compression leading to a progressive increase of current blockade. More interestingly, the signals have double peaks each: a current blockade followed to an enhancement during the polymer expulsion outside the nanochannel. This current enhancement could be attributed to the ion concentration modulation when the polymer get out of the channel[50,51]. For the semi-dilute regime, the translocation is carried out in a channel with similar pore diameters and cone angle (α = 1.57°). The current blockade events are found much more symmetrical (Figure 1f). The lack of a compression under similar nanopore size as in dilute regime can be assigned to the existence of a polymer matrix due to the overlap of coils. Indeed, under crowded environment the volume of a polymer chain is reduced. These observations agree with the theoretical studies of Daoud and de Gennes using a scaling method[52].

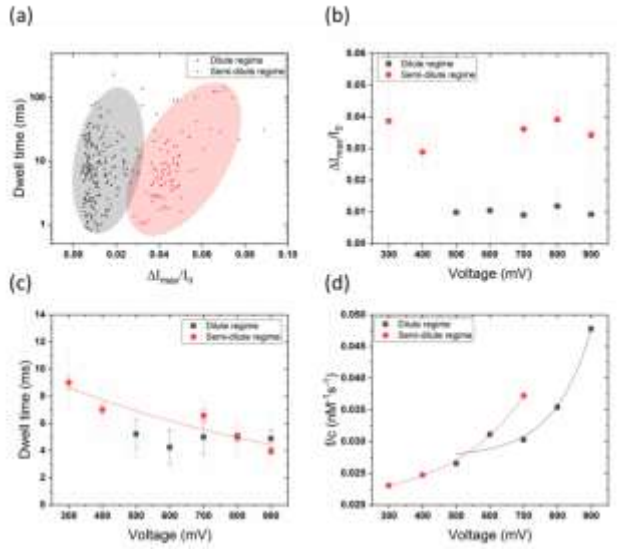

Fig. 2 (a) Event map for two regimes obtained under V = 700 mV. Blockade rate (b), dwell time (c) and frequency of events (d) of HA under dilute regime (black square) and semi-dilute regime (red circle) against applied voltage. Channel 1 in black: D_{base} = 715 nm, D_{tip} = 23.5 nm and Channel 2 in red: D_{base} = 750 nm, D_{tip} = 35.4 nm. The transparent error bars represent the full width at half maximum of the Gaussian distributions and the solid error bars represent the standard error. In Figure d, the lines are the exponential fitting of equation (3).

Figure 2a shows an event map of hyaluronic acid translocation in two regimes under 700 mV presenting two populations clearly. The different regimes of polymer solution induce in a different relative current blockade ratio $\Delta I_{max}/I_0$ (Figure 2b obtained from Figure S4 amd S5). The de Gennes' blob model has been used to describe flexible polymers in a long cone-shaped channel by Nikoofard and Fazli[34,52]. The linear density of the monomers along the channel axis *x* can be written as:

$$\lambda(x) \sim \frac{1}{b}\left(\frac{\xi(x)}{b}\right)^{\frac{1}{\nu}-1} \quad (1)$$

where *b* is the monomer size, $\frac{1}{\nu} - 1$ equals to 0.7 as the Flory component ν equals to 0.6 in this case[34,53] and ξ(x) is the blob size: $\xi(x) \sim D_0 + 2(x+a)\tan\alpha$. D_0 is the pore diameter of the tip side, α is the channel apex angle and a is the distance between beginning of the channel and the position of molecule beginning that can be fixed to 0. Thus, by integrating $\lambda(x)$ along the distance *L* occupied by polymer in the channel, we can get the total number of the polymer *N* as:

$$N \sim \frac{b^{-\frac{1}{\nu}}}{\tan\alpha}\left[(D_0 + 2(a+L)\tan\alpha)^{\frac{1}{\nu}} - (D_0 + 2a\tan\alpha)^{\frac{1}{\nu}}\right]. \quad (2)$$

From the equation 2, we can calculate *L* for hyaluronic acid in nanochannel 1 setting molar mass at 1.65 Mg mol^{-1}, $\tan\alpha$ at 0.027, D_0 at 23.5 nm, *b* at 0.75 nm^3 and a at 0. The *L* is obtained as 81 nm. Thus we can determine a circular frustum section with D_{small}=23.5 nm, L=81 nm, D_{large}=27.8 nm and *V*= 41953 nm^3. Then, the ratio η of the volume occupied by the hyaluronic acid in this section can be calculated to be 7.7% using 1.1 nm as the length of a disaccharide unit, 4350 as number of monomers and 0.68 nm^2 as the cross section of polymer chain ($V_{polymer}$=3254 nm^3). If we consider now that the channel contains two parts: one section is filled with one polymer and one section is full of electrolyte solution, we can define the nanochannel as a sum of two resistances R_1 which contains the HA and R_2 (Figure S3).

As the electrolyte solution has a NaCl concentration as high as 1 M, we neglect the conductance contribution of electrical double layer in the channel and the charge density of hyaluronic acid screened. Considering 7.7 % of the volume occupied by the molecule in R_1, the relative current blockade $\Delta G/G_0 = \Delta I/I_0$ is calculated to be 1.16 % (Figure S3). This value is quite close to average experimental data at about 1 % as shown in Figure 2b. As the channel has a length of 13 µm and a D_{Base} of 715 nm, we cannot claim that only one molecule is inside the channel. However the relative good agreement $\Delta G/G_0$ between calculation and experiment let think that in such dilute regime, only one molecule is strongly confined close to the tip side leading to the unique contribution of current blockade. Other hyaluronic acid molecules could be located in the channel but they are too far from the tip aperture and not compressed enough to contribute to the current blockade considering the large gyration diameter of HA. Therefore the de Gennes' blob model as well as the calculation by Fazli et al.[34,53] are perfectly suitable in the case of polymer translocation under dilute regime. If we do the

same calculation in the case of a semi-dilute regime, 0.7% of conductance decrease is obtained. This value is far from experimental one from 3% to 4%. This can be explained by the polymer matrix that fills the channel and takes more space inside.

Now, we investigate the dynamic aspects of HA translocation through conical nanochannel. The dwell time of translocations in two regimes in responding applied voltage increase is given Figure 2c. In the semi-dilute regime, the dwell time decreases exponentially in with the voltage. The exponential dependence can be described by the function $f(V) = Aexp(-V/V_c)$ where A = 12074 µs and V_c = 900 mV. This means that the dwell time measured in the semi-dilute regime could be considered as a transport time. It has been found by Oukhaled et al. that the dwell time of translocation of poly(ethylene glycol) chains (>35 kDa) in the semi-dilute regime is governed by the reptation time in a protein pore with small aspect ratio. It means that the extraction of one single chain of the polymer network into a small protein takes more time than the transport time[41]. This is contrary to our case where the nanochannel length scale is much larger than the polymer size. The reptation time of the polymer being extracted from the matrix is relatively short compared to the transport time. So this procedure is highly dependent on aspect ratio of the nanopore/nanochannel. In dilute regime, dwell time keeps almost constant when the electrical bias increases until to 900 mV.

Then we compare translocations in two regimes in terms of energy. This difference of free energy barrier can be obtained from the frequency of blockade events as a function of applied voltage according to Van't Hoff-Arrhenius law reading:

$$f = f_0 \exp\left[-\frac{V}{V_0}\right], \quad (3)$$

where f_0 is the frequency of blockades without applied electric bias

$$f_0 = k\frac{CDA}{L} exp\left[-\frac{U}{k_B T}\right], \quad (4)$$

where, k is a probability factor, C the polymer concentration, D the diffusion coefficient, A the cross-section area of the channel, L the channel length, $k_B T$ are the Boltzmann constant and the temperature and U the energy barrier. By fitting the data in Figure 2d with equation (3), f_0/C is obtained as 5.8 10^{-6} Hz nM^{-1} for dilute regime and 6.8 10^{-4} Hz nM^{-1} for the semi-dilute regime. The calculation of the absolute value is relatively uncertain because of the lack of precise values for k, L and D[40]. Thus, we can calculate the difference of activation energy by removing these factors and assuming the same diffusion coefficient:

$$\frac{f_{0\,D}/C_D}{f_{0\,SD}/C_{SD}} = \exp\left[\frac{U_{SD}-U_D}{k_B T}\right]. \quad (5)$$

$U_{SD} - U_D$ is obtained as -0.16$k_B T$. The value is still not precise because the diffusion coefficient of HA is not the same in two regimes (D_{SD} is slightly smaller than D_D). However the qualitative relation remains the same meaning as the energy barrier of translocation of hyaluronic acid through conical nanochannel in dilute regime is higher than that in semi-dilute regime. Comparing these two regimes, the confinement energy of the polymer stretching in the elongation shear is relatively low because of the stretch conformation of polymers in the network of the semi-dilute regime. For dilute regime, the required energy to deform the large polymer coil under confined environment should be larger but it is still negligible when the pore angle is small[33]. Thus the different energy barriers could be explained by the friction between polymer coils and channel surface during the compression procedure to reach the tip aperture in such a long nanochannel. Thereof, the energy from the interaction with the surface becomes dominant.

Influence of the tip aperture on HA translocation through conical nanochannel.

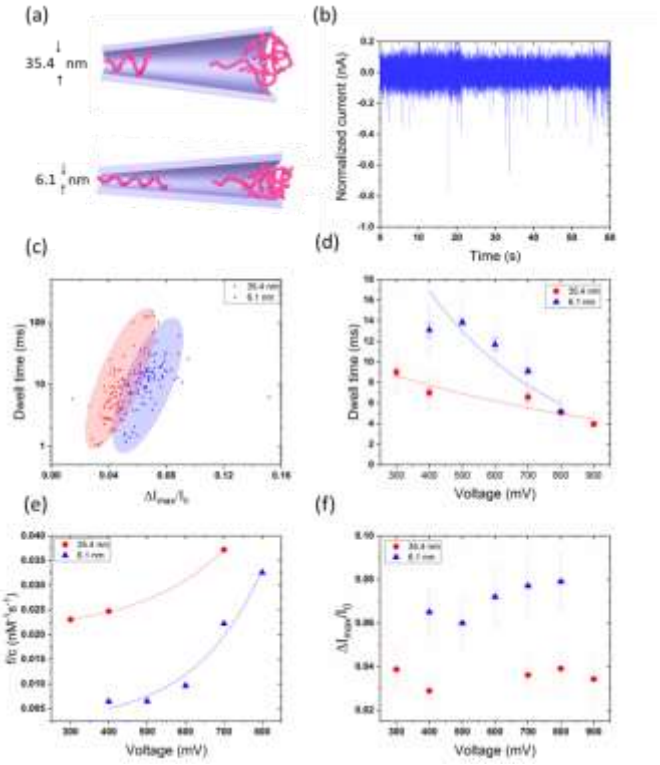

Fig. 3 (a) Sketches of hyaluronic acid translocation through long conical channel with different diameters. The sketches are not to scale. (b) Example of current trace for channel 3. (c) Event map for two channels under 400 mV. Dwell time (d) event frequency (e) and blockade rate (f) of HA in channel 2 (red circle) and in channel 3 (blue triangle) against applied voltage. Channel 2 in red: D_{base} = 750 nm, D_{tip} = 35.4 nm and channel 3 in blue: D_{base} = 1185 nm, D_{tip} = 6.1 nm. The transparent error bars represent the full width at half maximum of the Gaussian distributions and the solid error bars represent the standard error. In Figure e, the lines are the exponential fitting of equation (3).

Another key factor which influences polymer translocation is the nanochannel diameter. For our conical nanochannels, the tip diameter plays a more important role rather than the base due to the location of the sensing zone. First, we had to choose one regime for following investigations. When the polymer solution flows in the channel with the shrinking of the channel diameter, dilute solutions may be concentrated inside the channel into the semi-dilute regime. So to avoid this unexpected transition, we choose to conduct experiments under the same semi-dilute regime. To compare with the results obtained in the nanochannel 2 (D_{base} = 750 nm, D_{tip} =

35.4 nm α = 1.57°), we supply another set of experiments in nanochannel 3 (D_{base} =1185 nm and D_{tip} = 6.1 nm α = 2.59°) (Figure 3a). In this experiment set, the tip diameter is close to 2a of the hyaluronic acid molecule (where a is its persistence length with a value around 4 nm to 9 nm[54,55]).

Figure 3b shows a recorded current trace for nanochannel 3 and Figure 3c shows an event map for two channels under 400 mV. The dwell time in the channel of 35.4 nm seems shorter meanwhile its current blockade is higher than that in the channel of 6.1 nm. Details of dwell time as a function of applied voltage are shown in Figure 3d (obtained from Figure S5 amd S6). Translocation duration of HA in both two nanochannels follows exponential dependence ($f(V) = Aexp(-V/V_c)$ with A = 29731 µs, V_c = 578 mV for nanochannel of 6.1 nm and A = 11934 µs, V_c = 934 mV for nanochannel of 35.4 nm. This indicates that transport time has a dominating contribution to dwell time for the polyelectrolyte translocation in long conical nanochannel in the semi-dilute regime whatever the tip aperture diameter.

The difference of energy barrier between two nanochannels has been calculated by fitting event frequency as a function of applied voltage (Figure 3e). From this figure, we can see that the frequency of blockade events is higher for the larger nanochannel. From the equation (5), we calculate the difference of free energy barrier:

$$\frac{f_{0\ 35.4}/C_{35.4}}{f_{0\ 6.1}/C_{6.1}} = \exp\left[\frac{U_{6.1}-U_{35.4}}{k_BT}\right], \quad (6)$$

The value $U_{6.1} - U_{35.4}$ is obtained as $0.66k_BT$. Here, the higher energy barrier for the small nanopore can be assigned to the friction as the interaction between molecules and the nanochannel surface is strong. This difference of friction in two regimes could be explained by the scaling law of de Gennes using blob models. The ratio of frictional forces between two nanochannels can be described by the ratio of the effective monomer mobility B^{-1} that includes the hydrodynamic interactions between monomers in confined space. Thus according to Daoudi and Brochard[33], we have:

$$\frac{B_{6.1}^{-1}}{B_{35.4}^{-1}} = \frac{\eta_s(\xi_{6.1}/g_{6.1})}{\eta_s(\xi_{35.4}/g_{35.4})} \quad (7)$$

where η_s is the solution viscosity, for the semi-dilute regime, ξ is the mesh size of the polymer network, g the number of monomers inside a blob of diameter ξ[41]. This ratio can be simplified by substituting $g = \left(\frac{\xi}{a}\right)^{5/3}$ into Eq. (7) as:

$$\frac{B_{6.1}^{-1}}{B_{35.4}^{-1}} = \left(\frac{\xi_{35.4}}{\xi_{6.1}}\right)^{2/5} \quad (8)$$

The ξ is calculated using $\xi = a\varphi^{-0.75}$ with a of 1 nm and φ the volume fraction of polymers. Assuming that hyaluronic acid has similar density of water, we could write φ =c. The volume fraction of a polymer in confined nanochannel (close to tip) can be obtained by calculating the distance L occupied by the molecule in nanochannel using equation (2). For the nanochannel with tip aperture of 6.1 nm, its blob diameter ξ is obtained to be 3.6 nm as volume fraction is 18.4%; for the nanochannel with tip aperture of 35.4 nm, its blob diameter ξ is obtained to be 9.8 nm as volume fraction is 4.8%. Therefore, the friction coefficient in nanochannel of 6.1 nm is higher than in nanochannel of 35.4 nm. This is in accordance with the different energy barriers obtained previously that reduction of tip aperture of nanochannels will increase the frictions between polymers and the channel wall leading to a higher energy barrier. This difference in volume fraction due to the occupation of the polymer close to the tip aperture (18.4% for nanochannel of 6.1 nm and 4.8% for nanochannel of 35.4 nm) can also well explain the difference of current blockade rates in Figure 3f: with more occupation by the polymer, it has a higher current drop. So the equation (2) and (7) based on scaling law can be a good tool to predict quantitatively or qualitatively the translocation of large flexible polyelectrolytes through a long conical nanochannel.

Detection of HA with nanochannels decorated with enzyme in tip.

After studying the polymer translocation through our conical nanochannels, we performed experiments involving grafted enzymes. Besides the shape controllability, PET track-etched nanochannels have also advantages on simplicity of surface modification due to carboxylic acid moieties. In the first set of experiments, we use conical nanochannel of D_{base}=1000 nm, D_{tip}=4.3 nm, α = 2.19° (noted nanochannel 4). The hyaluronidase was grafted using EDC under MES buffer by addition on base side. The chemical grafting lasts for the whole night to assure a maximum enzyme immobilization. Regarding to the size of the tip diameter (4.3 nm smaller than the size of enzyme), we can assume that enzymes fill the nanopore but do not reach the tip end. After being washed and stabilized by PBS buffer, the functionalized nanochannel was used for hyaluronic acid translocation experiments. We notice that we used in the same condition as the previous experiment performed in the semi-dilute regime.

Figure 4a is a schematic representation of enzymes immobilized in the nanochannel with small tip diameter. After enzymes immobilization, a slight diminution of effective channel diameter was measured (Figure S7) due to steric block of hyaluronidase close to the tip side of the nanopore. This allows confirming the success of functionalization. Effective tip diameter becomes 2.2 nm instead of 4.3 nm of the channel without enzymes resulting in higher amplitude of relative current blockade (Figure 4c). Sporadic attachment of hyaluronidase is suggested in the light of the crosslinking conditions[4]. The HA driven into the channel by electrical bias will be bound and hydrolyzed by hyaluronidase, thus we could expect that more events will be detected. The experimental results show that translocation frequency gets an increase of a factor about 20 compared to the experiment in the channel of 6.1 nm without enzymes (Figure 4d and Figure 3e). We also observe a larger distribution of relative current blockades meaning that varieties of chain length are recorded (Figure 4 and Figure S8). In addition, dwell times recorded here are much shorter than those of un-degraded HA because the degraded polymers are shorter (Figure 4e). With this base-hyaluronidase-functionalized nanochannel, it could be possible to analyze the size distributions as of the enzymatic reaction products in real time after a calibration. The successful detection of enzymatic degradation products by immobilized hyaluronidase confirms that it remains reactivity after crosslinking conditions, under confinement and electrical bias. This evidence can allow us to further observe the direct interaction between HA and enzymes in order to measure the

duration of the intermediate complexion at single molecule level in our channel.

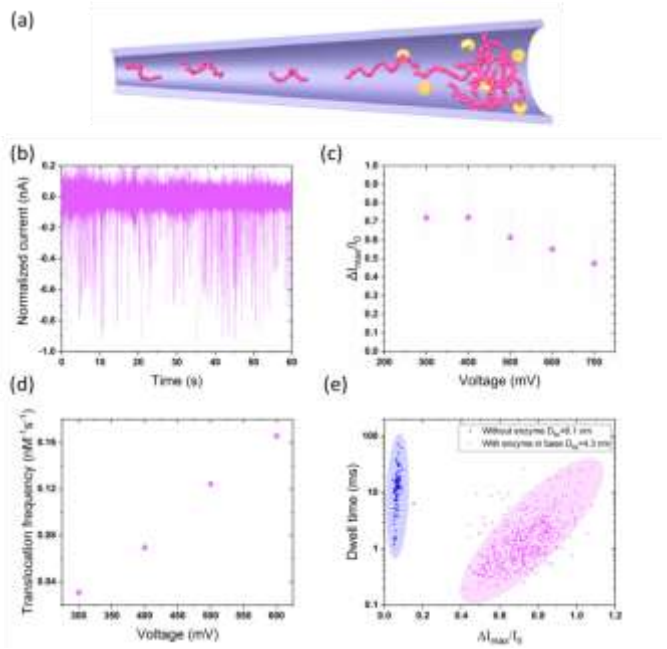

Fig. 4 (a) Sketch of hyaluronic acid flowing into the long conical channel with hyaluronidase immobilized on the base side. The sketch is not to scale. (b) Example of a current trace recorded. Frequency (c), dwell time (d) and blockade rate (e) of translocation events against applied voltage. Channel 4: D_{base}=1000 nm, D_{tip}=4.3nm. The transparent error bars represent the full width at half maximum of the Gaussian distributions and the solid error bars represent the standard error.

Detection of HA-Hyaluronidase interaction with nanochannels decorated with enzyme in base.

To do so, we functionalized the nanochannel 2 (D_{tip} =35.4 nm) with hyaluronidase following the same procedure as the one used for nanochannel 4 previously. The current-voltage curves before and after enzyme grafting was measured in PBS, 1M NaCl also showing clear reduction of the tip size and surface charge (Figure S9). This can be an evidence of the successful enzyme grafting inside the nanochannel. According to the large tip diameter, enzyme can be located on the tip entrance. The translocation experiments in the semi-dilute regime were repeated in this nanochannel and impressive long events were observed for the first time in our work (Figure 5a). The current trace show several events with mean duration of 1022 ± 78 ms. Compared to our previous experiments, no relationship between the event duration and applied voltages was found indicating a static behavior of the polymer instead of a kinetic process. In addition, the duration of about 1 s is in agreement with a enzymatic reaction time scale usually reported between some hundreds milliseconds to several seconds[56]. Thus, these long events can be assigned to the enzymatic reactions between hyaluronic acid and hyaluronidase. More interestingly, some peaks inside these long blockades were observed as shown in Figure 5a. This could be explained by the presence of another HA that passes through the nanochannel when a polymer is bound to the enzyme. The dwell time of this peak is longer than the events without enzymes. This should be due to the reduction of the channel diameter by enzymes and/or interactions between polymers and enzymes. To confirm the origin of these two kinds of events, we have added a hyaluronidase inhibitor (quercetin) to the tip side of the channel and then we continue to record the current traces. After addition of quercetin, long events (second time scale) have not been recorded but only short ones (tens millisecond time scale). As shown in Figure 5b, these events have very similar shape, amplitudes and duration of the peak inside long current blockade. This result confirms our assumption that the long events can be assigned to the specific binding of substrate-enzyme and the short one to the passage of the polymer chain when an enzyme is working. This draws a very clear image describing what is going on in the channel when an enzyme is grafted inside. Thus, for first time, a direct measurement of off-rate duration of enzymatic reaction is achieved at single molecule level under condition commonly used in membrane science for enzymatic reactor membrane.

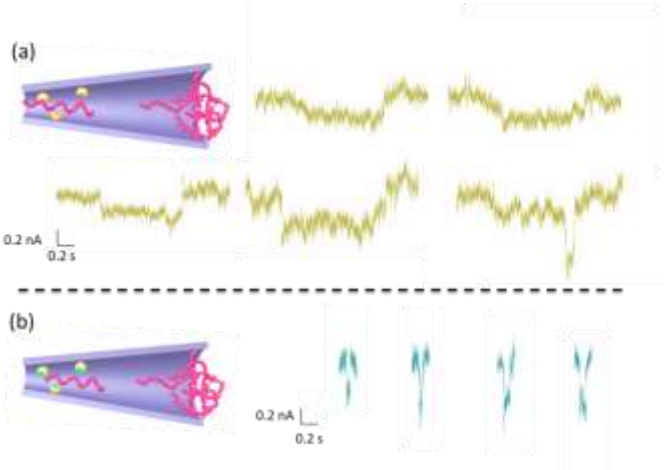

Fig. 5 (a) Sketch of translocating hyaluronic acid through the channel 2 with hyaluronidase in the tip side and examples of current blockades. (b) Sketch of translocating hyaluronic acid through the channel 3 with inhibited hyaluronidase in the tip side and examples of current blockades. The sketches are not to scale.

Conclusions

The translocation of hyaluronic acid with a molar weight at about 1.5 to 1.8 MDa was directly observed for the first time through a conical nanochannel using resistive pulse technique. The inner-channel behaviors can be well explained by the de Gennes's scaling theory. We studied the effect of the solution regime (dilute and semi-dilute) and pore diameter to better understand how these conditions control the transport and the polymer conformation inside the narrow aperture of the nanopore. Conversely than protein pores, the conical nanochannel the surface energy is predominant than the confinement. Then, hyaluronidase was immobilized inside the conical nanochannel for characterizing degradations of hyaluronic acid. Playing with the nanochannel diameter, a real time analyze of degradation products can be feasible after a

simple calibration. Finally, by grafting the enzymes at the tip side of a larger nanochannel, the duration of enzyme-substrate intermediate complex was measured for the first time under confinement at single molecule scale. This work opens a new gate in three distinct research and application fields. Firstly, the direct observation and validation of theory of polymers inside conical nanochannel will allow answering numerous questions in basic description of polymer translocation. We can expect that it will help the membrane design involving polymer filtration application. Secondly, the nanochannel is a suitable platform to investigate protein-protein/molecule interactions at single molecule level. Lastly, the nanochannel can provide answers to questions related to the impact of immobilization and the confinement on enzymatic activity. We can expect that this new approach to characterize individual enzymatic reactions will help researchers to understand the involvement of confinement on enzymatic degradation. This will allow optimizing the enzymatic grafting in numerous applications in material or membrane science.

Conflicts of interest

There are no conflicts to declare.

Acknowledgements

Single tracks have been produced in GANIL (Caen, France) in the framework of an EMIR project. The authors acknowledge Pr. E. Balanzat (CIMAP/Caen) for the assistance during swift heavy ion irradiation.

Notes and references

1. Kirk, O., Borchert, T. V. & Fuglsang, C. C. Industrial enzyme applications. *Curr. Opin. Biotechnol.* **13**, 345–351 (2002).
2. Rios, G. M., Belleville, M. P., Paolucci, D. & Sanchez, J. Progress in enzymatic membrane reactors – a review. *J. Memb. Sci.* **242**, 189–196 (2004).
3. Coglitore, D., Janot, J.-M. & Balme, S. Protein at liquid solid interfaces: Toward a new paradigm to change the approach to design hybrid protein/solid-state materials. *Adv. Colloid Interface Sci.* **270**, 278–292 (2019).
4. Hanefeld, U., Cao, L. & Magner, E. Enzyme immobilisation: fundamentals and application. *Chem. Soc. Rev.* **42**, 6211–6212 (2013).
5. Luckarift, H. R., Spain, J. C., Naik, R. R. & Stone, M. O. Enzyme immobilization in a biomimetic silica support. *Nat. Biotechnol.* **22**, 211–213 (2004).
6. Kim, J., Grate, J. W. & Wang, P. Nanostructures for enzyme stabilization. *Chem. Eng. Sci.* **61**, 1017–1026 (2006).
7. Bouaziz, Z. *et al.* Structure and antibacterial activity relationships of native and amyloid fibril lysozyme loaded on layered double hydroxide. *Colloids Surfaces B Biointerfaces* **157**, 10–17 (2017).
8. Md Jani, A. M., Losic, D. & Voelcker, N. H. Nanoporous anodic aluminium oxide: Advances in surface engineering and emerging applications. *Prog. Mater. Sci.* **58**, 636–704 (2013).
9. Chang, S.-F., Chang, S.-W., Yen, Y.-H. & Shieh, C.-J. Optimum immobilization of Candida rugosa lipase on Celite by RSM. *Appl. Clay Sci.* **37**, 67–73 (2007).
10. Zucca, P., Fernandez-Lafuente, R. & Sanjust, E. Agarose and its derivatives as supports for enzyme immobilization. *Molecules* **21**, 1577 (2016).
11. Ndour, N. *et al.* Impact of polyelectrolytes on lysozyme properties in colloidal dispersions. *Colloids Surfaces B Biointerfaces* **183**, 110419 (2019).
12. Gkaniatsou, E. *et al.* Metal–organic frameworks: a novel host platform for enzymatic catalysis and detection. *Mater. Horizons* **4**, 55–63 (2017).
13. Mehta, J., Bhardwaj, N., Bhardwaj, S. K., Kim, K.-H. & Deep, A. Recent advances in enzyme immobilization techniques: Metal-organic frameworks as novel substrates. *Coord. Chem. Rev.* **322**, 30–40 (2016).
14. Michaelis, L. & Menten, M. Kinetik der Invertinwirkung. *Biochem. Z.* **49**, 333–369 (1913).
15. Xie, X. S. Enzyme Kinetics, Past and Present. *Science (80-.).* **342**, 1457 LP-1459 (2013).
16. Xie, X. S. & Trautman, J. K. OPTICAL STUDIES OF SINGLE MOLECULES AT ROOM TEMPERATURE. *Annu. Rev. Phys. Chem.* **49**, 441–480 (1998).
17. Funatsu, T., Harada, Y., Tokunaga, M., Saito, K. & Yanagida, T. Imaging of single fluorescent molecules and individual ATP turnovers by single myosin molecules in aqueous solution. *Nature* **374**, 555–559 (1995).
18. Neuman, K. C. & Nagy, A. Single-molecule force spectroscopy: optical tweezers, magnetic tweezers and atomic force microscopy. *Nat. Methods* **5**, 491 (2008).
19. Sakmann, B. *Single-Channel Recording*. (Springer US, 2013).
20. Kherim, W., Veerle, V. M., Carsten, W. & Giovanni, M. Single-molecule nanopore enzymology. *Philos. Trans. R. Soc. B Biol. Sci.* **372**, 20160230 (2017).
21. Fennouri, A. *et al.* Kinetics of enzymatic degradation of high molecular weight polysaccharides through a nanopore: Experiments and data-modeling. *Anal. Chem.* **85**, 8488–8492 (2013).
22. Fennouri, A. *et al.* Single Molecule Detection of Glycosaminoglycan Hyaluronic Acid Oligosaccharides and Depolymerization Enzyme Activity Using a Protein Nanopore. *ACS Nano* **6**, 9672–9678 (2012).
23. Giamblanco, N. *et al.* Amyloid Growth, Inhibition, and Real-Time Enzymatic Degradation Revealed with Single Conical Nanopore. *Anal. Chem.* **90**, 12900–12908 (2018).
24. Ma, T., Balanzat, E., Janot, J.-M. & Balme, S. Single conical track-etched nanopore for a free-label detection of OSCS contaminants in heparin. *Biosens. Bioelectron.* **137**, 207–212 (2019).
25. Wei, R., Gatterdam, V., Wieneke, R., Tampé, R. & Rant, U. Stochastic sensing of proteins with receptor-modified solid-state nanopores. *Nat. Nanotechnol.* **7**, 257 (2012).
26. Yusko, E. C. *et al.* Controlling protein translocation through nanopores with bio-inspired fluid walls. *Nat. Nanotechnol.* **6**, 253 (2011).

27. Shi, X. *et al.* Dynamics of a Molecular Plug Docked onto a Solid-State Nanopore. *J. Phys. Chem. Lett.* **9**, 4686–4694 (2018).
28. De Gennes, P. G. Scaling concepts in polymer physics. Cornell university press. *Ithaca N.Y.,* 324 (1979).
29. Odijk, T. The statistics and dynamics of confined or entangled stiff polymers. *Macromolecules* **16**, 1340–1344 (1983).
30. Hydrodynamics of linear macromolecules . *Pure and Applied Chemistry* **12**, 563 (1966).
31. De Gennes, P. G. Coil ‐ stretch transition of dilute flexible polymers under ultrahigh velocity gradients. *J. Chem. Phys.* **60**, 5030–5042 (1974).
32. Pincus, P. Excluded Volume Effects and Stretched Polymer Chains. *Macromolecules* **9**, 386–388 (1976).
33. Daoudi, S. & Brochard, F. Flows of Flexible Polymer Solutions in Pores. *Macromolecules* **11**, 751–758 (1978).
34. Colby, R. H. & Rubinstein, M. Polymer physics. *New-York Oxford Univ.* **100**, 274 (2003).
35. Nikoofard, N., Khalilian, H. & Fazli, H. Directed translocation of a flexible polymer through a cone-shaped nano-channel. *J. Chem. Phys.* **139**, 74901 (2013).
36. Li, L., Chen, Q., Jin, F. & Wu, C. How does a polymer chain pass through a cylindrical pore under an elongational flow field? *Polymer (Guildf).* **67**, A1–A13 (2015).
37. Dekker, C., Article, R. & Dekker, C. Solid-state nanopores. *Nat. Nanotechnol.* **2**, 209–215 (2007).
38. Kasianowicz, J. J., Brandin, E., Branton, D. & Deamer, D. W. Characterization of individual polynucleotide molecules using a membrane channel. *Proc. Natl. Acad. Sci. U. S. A.* **93**, 13770–3 (1996).
39. Johnson, K. A. & Goody, R. S. The Original Michaelis Constant: Translation of the 1913 Michaelis–Menten Paper. *Biochemistry* **50**, 8264–8269 (2011).
40. Henrickson, S. E., Misakian, M., Robertson, B. & Kasianowicz, J. J. Driven DNA Transport into an Asymmetric Nanometer-Scale Pore. *Phys. Rev. Lett.* **85**, 3057–3060 (2000).
41. Oukhaled, A. G., Biance, A. L., Pelta, J., Auvray, L. & Bacri, L. Transport of long neutral polymers in the semidilute regime through a protein nanopore. *Phys. Rev. Lett.* **108**, (2012).
42. Steinbock, L. J., Lucas, A., Otto, O. & Keyser, U. F. Voltage-driven transport of ions and DNA through nanocapillaries. *Electrophoresis* **33**, 3480–3487 (2012).
43. Bell, N. A. W., Muthukumar, M. & Keyser, U. F. Translocation frequency of double-stranded DNA through a solid-state nanopore. *Phys. Rev. E* **93**, 22401 (2016).
44. Bell, N. A. W., Chen, K., Ghosal, S., Ricci, M. & Keyser, U. F. Asymmetric dynamics of DNA entering and exiting a strongly confining nanopore. *Nat. Commun.* **8**, 380 (2017).
45. Harrell, C. C. *et al.* Resistive-Pulse DNA Detection with a Conical Nanopore Sensor. *Langmuir* **22**, 10837–10843 (2006).
46. Apel, P. Track etching technique in membrane technology. *Radiat. Meas.* **34**, 559–566 (2001).
47. Cowman, M. K., Schmidt, T. A., Raghavan, P. & Stecco, A. Viscoelastic Properties of Hyaluronan in Physiological Conditions. *F1000Research* **4**, 622 (2015).
48. Balme, S., Lepoitevin, M., Dumée, L. F., Bechelany, M. & Janot, J.-M. Diffusion dynamics of latex nanoparticles coated with ssDNA across a single nanopore. *Soft Matter* **13**, 496–502 (2017).
49. Cabello-Aguilar, S. *et al.* Dynamics of polymer nanoparticles through a single artificial nanopore with a high-aspect-ratio. *Soft Matter* **10**, 8413–8419 (2014).
50. Goyal, G., Freedman, K. J. & Kim, M. J. Gold Nanoparticle Translocation Dynamics and Electrical Detection of Single Particle Diffusion Using Solid-State Nanopores. *Anal. Chem.* **85**, 8180–8187 (2013).
51. Chen, K. *et al.* Biphasic Resistive Pulses and Ion Concentration Modulation during Particle Translocation through Cylindrical Nanopores. *J. Phys. Chem. C* **119**, 8329–8335 (2015).
52. Daoud, M. & De Gennes, P. G. Statistics of macromolecular solutions trapped in small pores. *J. Phys. Fr.* **38**, 85–93 (1977).
53. Nikoofard, N. & Fazli, H. A flexible polymer confined inside a cone-shaped nano-channel. *Soft Matter* **11**, 4879–4887 (2015).
54. Buhler, E. & Boué, F. Chain Persistence Length and Structure in Hyaluronan Solutions: Ionic Strength Dependence for a Model Semirigid Polyelectrolyte. *Macromolecules* **37**, 1600–1610 (2004).
55. Cleland, R. L. The persistence length of hyaluronic acid: An estimate from small-angle X-ray scattering and intrinsic viscosity. *Arch. Biochem. Biophys.* **180**, 57–68 (1977).
56. Toni, T. The Machinery of Life: David S. Goodsell 2nd edn., 2009 Springer-Verlag, London. *Hum. Genomics* **4**, 369 (2010).